# Spectrum Design for Orthogonal Chirp Division Multiplexing Transmissions

Muhammad Shahmeer Omar<sup>®</sup>, Graduate Student Member, IEEE, and Xiaoli Ma

Abstract—Orthogonal chirp division multiplexing (OCDM) is a spread spectrum technique that leverages the orthogonality of cyclically shifted linear chirp signals to maximize spectral efficiency. However, since each chirp spans the entire signal band, the only way to control its bandwidth is to alter the sampling rate of the digital-to-analog converter (DAC). This letter shows that the inherent relationship between the discrete Fresnel transform (DFnT) and the discrete Fourier transform (DFT) facilitates a simple method of designing the spectrum of the signal without adding significant complexity. This enables direct implementation of the digital filters proposed in literature for advanced waveforms. Subsequently, simulations corroborate the performance of the proposed method and filtered-OCDM (f-OCDM) in wireless multipath fading channels in comparison with orthogonal frequency division multiplexing (OFDM) with a given spectral mask.

*Index Terms*—Orthogonal chirp division multiplexing, OFDM, filtering, fifth generation (5G).

#### I. Introduction

RTHOGONAL frequency division multiplexing (OFDM) is the most widely used waveform today in wireless communications. Having been employed in long term evolution (LTE) standard, it will now be a core component of fifth generation (5G) networks as well. This is mostly because of its ease of implementation, availability of low complexity equalization algorithms and its resistance to multi-path fading. However, OFDM is known to cause significant out of band emissions (OOBE). As a result, there has been a significant push among industry and academia to explore filtered variants of OFDM [1] as future generations of wireless networks will see increasing amounts of traffic and lower tolerances for interference.

Popular contenders for filtered waveforms include filter bank multi-carrier (FBMC), which employs subcarrier level filtering, and universal filtered multi-carrier (UFMC) and filtered-OFDM (f-OFDM), which employ sub-band level filtering [2]–[6]. While each of these techniques addresses the OOBE problem in OFDM to varying degrees, they still use the parallel narrow band subchannels in OFDM which makes them susceptible to impairments such as narrow band interference

Manuscript received June 28, 2020; accepted July 15, 2020. Date of publication July 21, 2020; date of current version November 9, 2020. This work was supported in part by an Industry/University Cooperative Research Center of National Science Foundation Center on Fiber Wireless Integration and Networking (FiWIN) for heterogeneous mobile data communications under Contract 1539976. The associate editor coordinating the review of this article and approving it for publication was A. Liu. (Corresponding author: Muhammad Shahmeer Omar.)

The authors are with the School of Electrical and Computer Engineering, Georgia Institute of Technology, Atlanta, GA 30332 USA (e-mail: momar6@gatech.edu; xiaoli@gatech.edu).

Digital Object Identifier 10.1109/LWC.2020.3010774

(NBI) and deep fades which significantly impact the average performance.

As opposed to OFDM, orthogonal chirp division multiplexing (OCDM) employs a set of orthogonal chirps as carriers. Hence, each symbol is spread over the entire spectrum while preserving the spectral efficiency. Moreover, as shown in [7], OCDM transceivers have comparable complexity to that of OFDM due to their ability to employ the fast Fourier transform (FFT) and single-tap frequency domain equalization (FDE). The study also showed that when armed with minimum mean squared error (MMSE) or iterative block decision-feedback equalizers (IBDFE), OCDM performs better than OFDM in multipath channels and is more robust to interference caused by insufficient guard intervals [7].

The performance of OCDM was analyzed for coherent optical fiber systems in [8] and data rates of up to 112 Gbps were experimentally demonstrated using OCDM with intensity modulation and direct detection in [9]. A linear frequency modulation based channel estimation technique was proposed for OCDM in [10]. The performance of OCDM was analyzed for millimeter wave fiber-wireless networks using simulation and experimental results in [11] and it was shown that OCDM performs better than OFDM in the presence of NBI. In [12], a precoding scheme was proposed to enable full diversity transmission with reduced decoding complexity for OCDM multi-user uplink transmissions.

None of the aforementioned studies address spectral containment for OCDM, i.e., the signal being studied occupies the entire bandwidth between  $-f_s/2$  and  $f_s/2$ , where  $f_s$  is the sampling rate. Hence, so far, the only way to modify the bandwidth occupied by the signal is to alter the sampling rate. In this letter, we propose a simple method to flexibly design the spectrum of the OCDM signal by leveraging the relationship between the discrete Fresnel transform (DFnT) and the discrete Fourier transform (DFT). There are three main advantages for doing this: first, OCDM transmissions are able to meet any spectral mask requirements without having to alter the sampling rates of the digital-to-analog converters (DAC), thus making any potential transition from OFDM to OCDM much easier. Second, OCDM signals can be used with the slot-based resource grid laid out in current standards because of its compatibility with OFDM and thus, avoid having to redesign the network. Third, the filters proposed for the advanced OFDMbased waveforms, like UFMC and f-OFDM, can be directly applied to OCDM to achieve better spectral containment and reduced OOBE.

The remainder of this letter is organized as follows. Section II introduces the linear chirps used in OCDM and sets up some mathematical preliminaries. Section III develops the spectrum control scheme for OCDM, Section IV presents

2162-2345 © 2020 IEEE. Personal use is permitted, but republication/redistribution requires IEEE permission. See https://www.ieee.org/publications/rights/index.html for more information.

the numerical results, and Section V presents the conclusions of this letter.

#### II. OCDM SYSTEM MODEL

The continuous time root chirp in OCDM is defined by

$$\phi_0(t) = e^{j\frac{\pi}{4}} e^{-j\pi \frac{N}{T^2}t^2}, \quad 0 \le t < T, \tag{1}$$

where T is the symbol period and  $N/T^2$  is the chirp rate. In order to preserve orthogonality, the other N-1 chirps are each delayed by an integer multiple of T/N. Hence, the chirps can be characterized by  $\phi_k(t) = \phi_0(t-k\frac{T}{N})$ , where  $k \in [0,N-1]$ . Assuming that N is even, it is then fairly easy to see that sampling at a rate of N/T results in the discrete chirp given by

$$\psi_k(n) = \phi_k(t) \Big|_{t=n\frac{T}{N}} = e^{j\frac{\pi}{4}} e^{-j\frac{\pi}{N}(n-k)^2}, \ \forall n, k \in [0, N-1].$$
 (2

For the remainder of this letter, we assume N to be even, keeping in mind that extending to the odd case is straightforward with minor appropriate modifications. Eq. (2) gives us the basis for the digital implementation of OCDM using the IDFnT as the transmitter kernel. Hence, the discrete time modulated signal is given by (see, [7])

$$x(n) = \sum_{k=0}^{N-1} u_k \psi_k(n),$$
 (3)

where  $u_k$  are symbols taken from a complex modulation alphabet such as quadrature amplitude modulation (QAM). In matrix-vector notation, this is equivalent to  $\mathbf{x} = \mathbf{\Phi}^{\mathcal{H}}\mathbf{u}$ , where  $\mathbf{\Phi}$  is an  $N \times N$  matrix whose  $k^{\text{th}}$  column is given by  $[\psi_k(0), \ \psi_k(1), \ , \dots, \ \psi_k(N-1)]^{\mathcal{H}}/\sqrt{N}$ , and  $(.)^{\mathcal{H}}$  denotes the conjugate transpose.

The continuous-time, interpolated chirp obtained from Eq. (2) is the periodic extension of the chirp defined in Eq. (1) and is given by

$$\phi_0'(t) = \begin{cases} \phi_0(t) & t \in \left[ -\frac{T}{2}, \frac{T}{2} \right), \\ \phi_0(t - cT) & t \in \left[ -\frac{T}{2} + cT, \frac{T}{2} + cT \right). \end{cases}$$
(4)

Thus, the  $k^{\rm th}$  chirp is given by  $\phi_k'(t) = \phi_0'(t-kT/N)\Pi_T(t)$ , where  $\Pi_T(t) = 1$  if  $0 \le t < T$  and 0, otherwise. This results in a signal whose spectrum spreads from  $-f_s/2$  to  $f_s/2$ , where  $f_s = N/T$ .

### III. OCDM SPECTRUM CONTROL

Following baseband processing, samples are converted into an analog signal using a DAC and passed through a low-pass filter which shapes the spectrum according to the requirements of the application. When the signal occupies a bandwidth equal to the sampling rate, as is the case for OCDM, the filter needs to have a smaller transition region which increases the implementation complexity. In order to avoid this, signals are designed so that their spectra are limited to a frequency below the Nyquist frequency, i.e.,  $f < |f_s/2|$ . In OFDM, this is done by introducing guard tones. This is not as straightforward for OCDM since each chirp spans the entire band.

#### A. Constraining the OCDM Bandwidth

Consider an OCDM signal with M chirps, where  $M \le N$  is even. Re-sampling this signal by a factor of N/M and interpolating limits its bandwidth to a frequency below the Nyquist frequency. Using frequency-domain zero padding (FDZP) to achieve this, the resulting signal is given by

$$\mathbf{x} = \mathbf{F}_N^{\mathcal{H}} \mathbf{T} \mathbf{F}_M \mathbf{\Phi}_M^{\mathcal{H}} \mathbf{u},\tag{5}$$

where  $\mathbf{F}_K$  is the  $K \times K$  DFT matrix whose  $(n,k)^{\mathrm{th}}$  entry is given by  $F_K(n,k) = 1/\sqrt{K}e^{-j\frac{2\pi}{K}nk}$ ,  $\Phi_M$  is the  $M \times M$  DFnT matrix, and  $\mathbf{T}$  is an  $N \times M$  matrix given by  $[\mathbf{I}_{M,l}^T \, \mathbf{0}_{(N-M) \times M} \, \mathbf{I}_{M,u}^T]^T$ , with  $\mathbf{I}_{M,l}$  and  $\mathbf{I}_{M,u}$  being the first and last M/2 columns of the  $M \times M$  identity matrix, respectively and  $(.)^T$  being the matrix transpose. Since  $\Phi_M^{\mathcal{H}}$  is a circulant matrix, it can be diagonalized by the (I)DFT matrices. The eigenvalues can be denoted by an  $M \times M$  diagonal matrix  $\Gamma_M$ , whose  $(k,k)^{\mathrm{th}}$  entry is given by

$$\Gamma_M(k,k) = e^{-j\frac{\pi}{M}k^2}.$$
(6)

Substituting  $\Phi_M^{\mathcal{H}} = \mathbf{F}_M^{\mathcal{H}} \mathbf{\Gamma}_M^{\mathcal{H}} \mathbf{F}_M$  into Eq. (5) gives

$$\mathbf{x} = \mathbf{F}_N^{\mathcal{H}} \mathbf{T} \mathbf{\Gamma}_M^{\mathcal{H}} \mathbf{F}_M \mathbf{u}. \tag{7}$$

Hence, interpolating the signal is akin to adding null subcarriers to a precoded OFDM system. Since  $\mathbf{T}^T\mathbf{T} = \mathbf{I}_M$ , it is fairly easy to see that there is no interference, which will formally be proven in the following sections. Furthermore, when M = N, the system becomes the original OCDM signal. For the remainder of this letter we refer to the signal given by Eq. (7) as constrained OCDM (c-OCDM).

While FDZP is a convenient and simple method to control the bandwidth of the c-OCDM signal, a natural question that follows is: What is the modulation kernel of c-OCDM? The underlying waveform can be defined by re-sampling the columns of the matrix  $\Phi_M^{\mathcal{H}}$  by a rational factor of N/M. Let  $c_l(n) = e^{j\frac{\pi}{4}}e^{-j\frac{\pi}{M}(n-l)^2}$  be the  $l^{\text{th}}$  chirp in an OCDM modulator with M chirps, i.e.,  $0 \le l < M$ . Re-sampling is achieved by interpolating by a factor of U, low-pass filtering and finally decimating by a factor D, where U/D = N/M.

The up-sampled chirp is given by

$$c'_{l}(n) = \begin{cases} c_{l}(n/U) & \text{if } n/U \text{ is an integer,} \\ 0 & \text{otherwise.} \end{cases}$$
 (8)

The up-sampled signal is passed through a low-pass filter, whose impulse response is given by

$$g(n) = \frac{1}{M} e^{-j\frac{\pi}{MU}n} \frac{\sin(\frac{\pi}{U}n)}{\sin(\frac{\pi}{MU}n)}.$$
 (9)

The filter output is given by

$$\tilde{c}_l(n) = g(n) \circledast c'_l(n) = \sum_{m=0}^{MU-1} c'_l(m)g((n-m)_{MU}),$$
 (10)

where  $\circledast$  and  $(.)_N$  denote the circular convolution and modulo-N operations, respectively. Finally, the modulation kernel for c-OCDM is given by decimating  $\tilde{c}_l(n)$  by a factor of D. Using

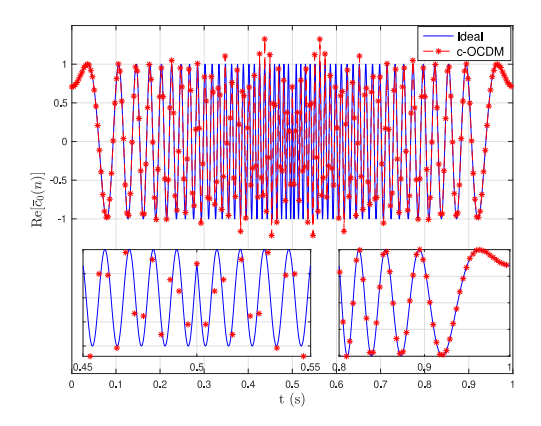


Fig. 1. Comparison of the c-OCDM modified root chirp, given by Eq. (11), where l=0, and a reference chirp.

Eqs. (8)–(10) and noting that D = UM/N, the modified chirp is given by

$$\bar{c}_{l}(n) = \frac{1}{M} e^{j\frac{\pi}{4}} \sum_{m=0}^{M-1} e^{-j\frac{\pi}{M}(m-l)^{2}} e^{-j\frac{\pi}{M}\left(\frac{M}{N}n-m\right)_{M}} \times \frac{\sin\left(\pi\left(\frac{M}{N}n-m\right)_{M}\right)}{\sin\left(\frac{\pi}{M}\left(\frac{M}{N}n-m\right)_{M}\right)}.$$
(11)

It is fairly easy to see that  $\bar{c}_l(n) = \psi_l(n)$  when M = N. Eq. (11) highlights the key difference between the OCDM and the proposed c-OCDM kernels. The c-OCDM is a distorted version of a chirp with a lower chirp rate. The distortion is caused by the sharp cut-off of the low-pass filter defined in Eq. (9). Fig. 1 plots the in-phase component of the root chirp in c-OCDM, given by  $\text{Re}[\bar{c}_0(n)]$ , where Re[.] denotes the real component of the complex argument, when M=200 and N=256. For reference, we also plot the corresponding ideal chirp with a normalized frequency span of  $[-\frac{M}{N}\pi, \frac{M}{N}\pi]$ . It can be seen that as long as the frequency is low, the c-OCDM chirp is the same as the ideal one. However, as the signal approaches the maximum frequency, the c-OCDM chirp samples deviate from the ideal chirp because of the Gibbs phenomenon.

#### B. Orthogonality of Modified Chirps

Let us define C as the  $N \times M$  modulation kernel matrix for c-OCDM, where the  $l^{\rm th}$  column is given by Eq. (11). From Eq. (7), it is easy to see that the kernel can be defined as

$$\mathbf{C} = \mathbf{F}_{N}^{\mathcal{H}} \mathbf{T} \mathbf{\Gamma}_{M}^{\mathcal{H}} \mathbf{F}_{M}, \tag{12}$$

where each column is a time-shifted version of the modified chirp  $\bar{c}_l(n)$ , as shown in Fig. 1. Now, let us define an  $M \times M$  matrix  $\mathbf{R} = \mathbf{C}^{\mathcal{H}}\mathbf{C}$ . By plugging in Eq. (12), we have

$$\mathbf{R} = \mathbf{C}^{\mathcal{H}} \mathbf{C} = (\mathbf{F}_{N}^{\mathcal{H}} \mathbf{T} \mathbf{\Gamma}_{M}^{\mathcal{H}} \mathbf{F}_{M})^{\mathcal{H}} \mathbf{F}_{N}^{\mathcal{H}} \mathbf{T} \mathbf{\Gamma}_{M}^{\mathcal{H}} \mathbf{F}_{M}$$

$$= \mathbf{F}_{M}^{\mathcal{H}} \mathbf{\Gamma}_{M} \mathbf{T}^{T} \mathbf{F}_{N} \mathbf{F}_{N}^{\mathcal{H}} \mathbf{T} \mathbf{\Gamma}_{M}^{\mathcal{H}} \mathbf{F}_{M}$$

$$= \mathbf{I}_{M}. \tag{13}$$

This proves that the columns of C are orthogonal.

#### C. Transceiver Design for c-OCDM

Consider c-OCDM transmissions in frequency-selective fading channels. A stream of bits is modulated and converted to a parallel block given by the length-M vector  $\mathbf{u}(i) = [u(iM), \ u(iM+1), \ , \ldots, \ u(iM+M-1)]^T$  and passed onto the c-OCDM modulator before a cyclic prefix (CP) of length  $N_{\rm g}$  is appended. Using Eq. (7), the modulated c-OCDM symbol is given by

$$\tilde{\mathbf{x}}(i) = \mathbf{T}_{\mathrm{CP}} \mathbf{F}_{N}^{\mathcal{H}} \mathbf{T} \mathbf{\Gamma}_{M}^{\mathcal{H}} \mathbf{F}_{M} \mathbf{u}(i), \tag{14}$$

where the resulting block contains  $N+N_{\rm g}$  samples. The matrix  $\mathbf{T}_{\rm CP}=[\mathbf{I}_{\rm CP}^T\ \mathbf{I}_N^T]^T$  is the CP insertion matrix, where  $\mathbf{I}_N$  and  $\mathbf{I}_{\rm CP}$  are the  $N\times N$  identity matrix and the last  $N_{\rm g}$  columns of  $\mathbf{I}_N$ , respectively. The block is subsequently serialized, passed through a DAC, filtered, amplified, and up-converted.

The channel is modeled as a finite impulse response (FIR) filter, with the impulse response given by  $\mathbf{h} = [h(0),\ h(1),\ ,\dots,\ h(L_{\rm h})]^T,$  where  $L_{\rm h}+1$  is the channel length. We assume that  $L_{\rm h} \leq N_{\rm g}$ , i.e., there is no inter-block interference. In addition, the received signal is also affected by additive white Gaussian noise (AWGN).

After down-conversion and serial-to-parallel conversion, the CP is removed and the resulting signal is given by

$$\mathbf{y}(i) = \mathbf{H}\mathbf{F}_{N}^{\mathcal{H}}\mathbf{T}\mathbf{\Gamma}_{M}^{\mathcal{H}}\mathbf{F}_{M}\mathbf{u}(i) + \mathbf{v}(i), \tag{15}$$

where **H** is an  $N \times N$  circulant matrix whose first column is given by  $[\mathbf{h}^T \ \mathbf{0}_{(N-L_{\rm h}-1)}^T]^T$ . Noting that each block is independent, we drop the block index from this point on. After conversion to the frequency domain and equalization, the block becomes

$$\bar{\mathbf{x}} = \mathbf{G}\mathbf{D}_h \mathbf{T} \mathbf{\Gamma}_M^{\mathcal{H}} \mathbf{F}_M \mathbf{u} + \mathbf{G}\mathbf{F}_N \mathbf{v}, \tag{16}$$

where  $\mathbf{D}_h = \mathbf{F}_N \mathbf{H} \mathbf{F}_N^{\mathcal{H}}$  is a diagonal matrix with the channel frequency response on its main diagonal and  $\mathbf{G}$  denotes the equalizer. We only consider linear MMSE equalization, which is represented by a diagonal matrix with the entries  $G(k) = \frac{H^{\star}(k)}{|H(k)|^2 + N_0/E_s}$  for  $k \in [0, N-1]$ , where H(k) is the  $k^{\text{th}}$  element of the CFR,  $E_s$  is the symbol energy, and  $N_0$  is the noise variance

The subset of frequency elements that contain data is then selected from the resulting block, phase corrected and converted back to the time domain. The resulting symbols are given by (see Eq. (16))

$$\hat{\mathbf{u}} = \mathbf{F}_{M}^{\mathcal{H}} \mathbf{\Gamma}_{M}^{\mathcal{H}} \mathbf{T}^{T} \mathbf{G} \mathbf{D}_{h} \mathbf{T} \mathbf{\Gamma}_{M}^{\mathcal{H}} \mathbf{F}_{M} \mathbf{u} + \mathbf{F}_{M}^{\mathcal{H}} \mathbf{\Gamma}_{M}^{\mathcal{H}} \mathbf{T}^{T} \mathbf{G} \mathbf{F}_{N} \mathbf{v}. \quad (17)$$

## D. Filtered-OCDM (f-OCDM)

We also consider filtered-OCDM (f-OCDM), for which the model is essentially the same as the one discussed previously except a digital filter is added to the transmitter, after parallel-to-serial conversion, and to the receiver before serial-to-parallel conversion. The filter has been adopted from [13], and its impulse response is given by

$$p_B(n) = \operatorname{sinc}\left(\frac{M + 2\delta_w}{N}n\right), \quad -\left\lfloor\frac{L_{\mathrm{f}}}{2}\right\rfloor \le n \le \left\lfloor\frac{L_{\mathrm{f}}}{2}\right\rfloor,$$

$$w(n) = \left(0.5\left(1 + \cos\left(\frac{2\pi n}{L_{\mathrm{f}} - 1}\right)\right)\right)^{0.6},$$

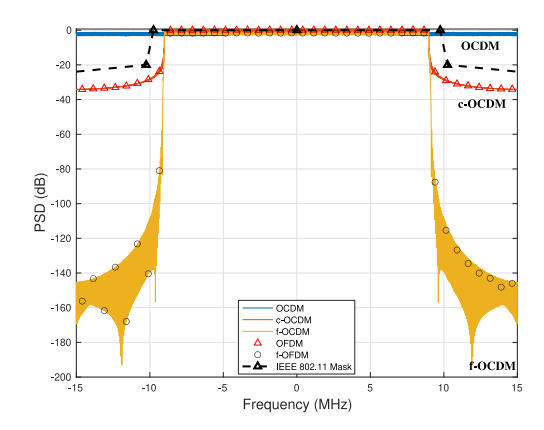


Fig. 2. Spectra of OCDM, c-OCDM, f-OCDM, OFDM and f-OFDM, and the IEEE 802.11 spectral mask.

$$f(n) = \frac{p_B(n)w(n)}{\sum p_B(n)w(n)},\tag{18}$$

where  $p_B(n)$  is the non-causal filter response, w(n) is the root-raised cosine window, f(n) is the overall filter impulse response,  $\delta_w$  denotes the excess bandwidth and  $L_{\rm f}-1$  is the filter order. It is pertinent to note that  $L_{\rm f}>N_{\rm g}$  which can cause inter-symbol-interference (ISI) as consecutive symbols start to overlap. However, when the filter pass-band width is large, this ISI coincides with the guard interval and hence, has a negligible effect on the performance.

#### IV. NUMERICAL RESULTS

In this section, we analyze the performance of the proposed c-OCDM and the subsequent extension to f-OCDM. For comparison, filtered OFDM (f-OFDM) and OCDM transmissions are also simulated. We consider only single user transmissions at a frequency of  $f_s = 30.72$  MHz, with N = 1024 and M = 600. This corresponds to a signal bandwidth of 18 MHz for OFDM, c-OCDM and their filtered counterparts. In OCDM, this translates to the use of only a subset of chirps that still occupies the entire band.

We assume that the channel remains static for one frame, which consists of three symbols, but changes randomly between frames. Each channel tap is modeled by an i.i.d complex Gaussian random variable with mean 0 and variance  $1/(L_{\rm h}+1)$ . Furthermore, the receiver is assumed to have perfect channel state information (CSI). Turbo codes with different code rates (R), as defined in LTE standard [14], are used for channel coding and all results are averaged over 10,000 channel and frame realizations.

Fig. 2 depicts the averaged spectra of the considered waveforms. As mentioned earlier, the OCDM signal occupies the entire band from  $-f_s/2$  to  $f_s/2$ . On the other hand, c-OCDM bandwidth is restricted to  $\alpha f_s$ , where  $\alpha = M/N$ . In fact, it can be seen that the c-OCDM and OFDM spectra are identical. Similarly, the spectra of the f-OFDM and f-OCDM are identical and exhibit a significant reduction in OOBE when compared to their unfiltered counterparts. For reference, the plot also shows the spectral mask for the 20 MHz channel in IEEE 802.11. In order to quantify OOBE performance, we

TABLE I ACPR COMPARISON

OFDM	f-OFDM	OCDM	c-OCDM	f-OCDM
-31.9  dB	-123.0  dB	0.3 dB	-31.8  dB	-123.0 dB

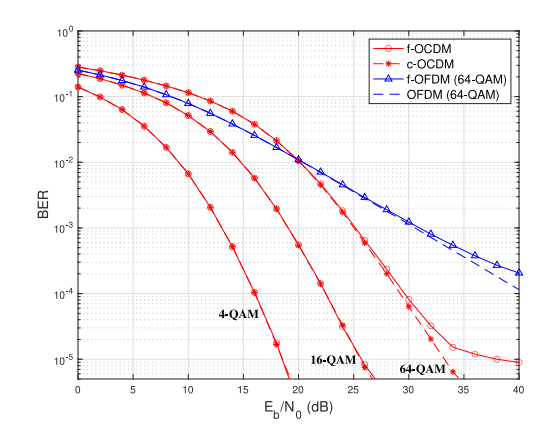


Fig. 3. Performance analysis of uncoded c-OCDM and f-OCDM for different constellations.

define the adjacent channel to peak ratio (ACPR) as

$$ACPR = \frac{E_{ob}}{E_{ib}}, \tag{19}$$

where  $E_{\rm ob} = \int_{f \in \overline{\mathcal{B}}} P(f) df$ ,  $E_{\rm ib} = \int_{f \in \mathcal{B}} P(f) df$ , P(f) is the power spectral density (PSD),  $\mathcal{B} = \{f: |f| \leq 10 \text{ MHz}\}$ , and  $\overline{\mathcal{B}} = \{f: |f| > 10 \text{ MHz}\}$ . Table I summarizes the values for ACPR, computed through simulations, for the considered waveforms.

We use the root-mean square error (RMSE) of the received data for the different schemes to verify the orthogonality of the modified chirps, which was theoretically proven in Eq. (13). The block-wise RMSE is given by

$$RMSE = \frac{\|\hat{\mathbf{u}} - \mathbf{u}\|}{\|\mathbf{u}\|}.$$
 (20)

Table II summarizes the average RMSE of the considered schemes for different signal-to-noise ratios (SNR). It can be seen that the RMSE for OCDM and c-OCDM are approximately the same for all SNR's, which implies that there is no additional ISI in c-OCDM. However, both f-OFDM and f-OCDM show higher RMSE at high SNR because of the distortion caused by the filter at the band edges.

Fig. 3 shows the average BER of c-OCDM and f-OCDM for different constellations. The performance of uncoded OFDM and f-OFDM is also included for reference. There are two important features that need to be highlighted: First, c-OCDM and f-OCDM depict identical performance for 4-QAM and 16-QAM transmissions, showing that the band-edge distortion caused by the filter is very minimal. Second, the graph shows that an error floor exists for f-OCDM and f-OFDM when 64-QAM is used. This error floor is caused by the distortion of the filter at the edges of the passband.

The performance of the considered schemes in the presence of channel coding is shown in Fig. 4, with different code rates and constellations. The first thing we notice is that the error floor we saw for 64-QAM in Fig. 3 disappears when

$\frac{E_b}{N_0}$ (dB)	RMSE					
	OCDM	c-OCDM	f-OCDM	f-OFDM		
10	0.357123281771521	0.356558576472204	0.356519089531401	0.356537755359865		
20	0.151028031207893	0.150202279104321	0.150392729025465	0.150448479679645		
30	0.0567129463028387	0.0561882167797665	0.0570450379674408	0.0570744485109061		
40	0.0199947232587626	0.0196413321247013	0.022428111600068	0.0224242994185006		
50	0.00672903486121301	0.00652437111331813	0.0126847959916717	0.012685172990502		

TABLE II
SYMBOL RMSE OF THE CONSIDERED SCHEMES

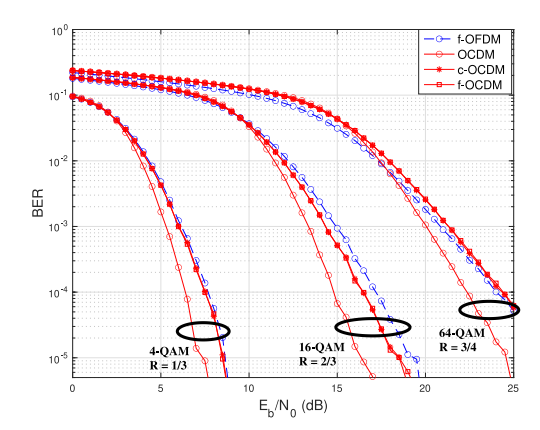


Fig. 4. Performance comparison of f-OCDM, c-OCDM, OCDM and f-OFDM with different code rates and modulation sizes.

channel coding is employed. Furthermore the performances of c-OCDM, OFDM and their filtered variants are identical, which is in contrast with the uncoded scenario, where the spreading scheme had the edge mainly due to the failure of uncoded OFDM to collect multipath diversity. However, channel coding changes that as both schemes exhibit diversity gains and hence, their performances converge. It can also be seen that OCDM outperforms c-OCDM. For example, at BER of  $10^{-4}$ , OCDM depicts a gain of approximately 1 dB for 16-QAM and 2 dB for 64-QAM transmissions, due to a greater spreading gain when compared to c-OCDM.

#### V. CONCLUSION

In this letter, we presented a simple method of digitally controlling the spectrum of the OCDM signal. We showed that this is equivalent to modulating using a modified chirp whose frequency span can be digitally controlled by padding zeros in the frequency domain. This was subsequently used to introduce digital filtering for OCDM, in order to further reduce its OOBE and make it more suitable for implementation in 5G and beyond networks. It was shown that restricting the bandwidth results in minor performance loss in multipath channels but allows for flexible spectrum design and additional filtering. In the future, we plan to analyze the performance of the

presented schemes in multi-user scenarios with synchronization errors. The performance of alternative filtering methods can also be considered.

#### REFERENCES

- [1] P. Banelli, S. Buzzi, G. Colavolpe, A. Modenini, F. Rusek, and A. Ugolini, "Modulation formats and waveforms for 5G networks: Who will be the heir of OFDM?: An overview of alternative modulation schemes for improved spectral efficiency," *IEEE Signal Process. Mag.*, vol. 31, no. 6, pp. 80–93, Nov. 2014.
- [2] F. Schaich and T. Wild, "Waveform contenders for 5G—OFDM vs. FBMC vs. UFMC," in *Proc. 6th Int. Symp. Commun. Control Signal Process. (ISCCSP)*, Athens, Greece, 2014, pp. 457–460.
- [3] H. Cho, Y. Yan, G. Chang, and X. Ma, "Asynchronous multi-user uplink transmissions for 5G with UFMC waveform," in *Proc. IEEE Wireless Commun. Netw. Conf. (WCNC)*, San Francisco, CA, USA, 2017, pp. 1–5.
- [4] D. Demmer, R. Zakaria, R. Gerzaguet, J. Doré, and D. Le Ruyet, "Study of OFDM precoded filter-bank waveforms," *IEEE Trans. Wireless Commun.*, vol. 18, no. 6, pp. 2889–2902, Jun. 2019.
- [5] X. Chen, L. Wu, Z. Zhang, J. Dang, and J. Wang, "Adaptive modulation and filter configuration in universal filtered multi-carrier systems," *IEEE Trans. Wireless Commun.*, vol. 17, no. 3, pp. 1869–1881, Mar. 2018.
- [6] J. Abdoli, M. Jia, and J. Ma, "Filtered OFDM: A new waveform for future wireless systems," in *Proc. IEEE 16th Int. Workshop Signal Process. Adv. Wireless Commun. (SPAWC)*, Stockholm, Sweden, 2015, pp. 66–70.
- [7] X. Ouyang and J. Zhao, "Orthogonal chirp division multiplexing," *IEEE Trans. Commun.*, vol. 64, no. 9, pp. 3946–3957, Sep. 2016.
- [8] X. Ouyang and J. Zhao, "Orthogonal chirp division multiplexing for coherent optical fiber communications," *J. Lightw. Technol.*, vol. 34, no. 18, pp. 4376–4386, Sep. 15, 2016.
- [9] X. Ouyang, G. Tall, M. Power, and P. Townsend, "Experimental demonstration of 112 Gbit/s orthogonal chirp-division multiplexing based on digital up-conversion for IM/DD systems with improved resilience to system impairments," in *Proc. Eur. Conf. Opt. Commun.*, Rome, Italy, 2018, pp. 1–3.
- [10] X. Ouyang, C. Antony, G. Talli, and P. D. Townsend, "Robust channel estimation for coherent optical orthogonal chirp-division multiplexing with pulse compression and noise rejection," *J. Lightw. Technol.*, vol. 36, no. 23, pp. 5600–5610, Dec. 01, 2018.
- [11] F. Lu, L. Cheng, M. Xu, J. Wang, S. Shen, and G. K. Chang, "Orthogonal chirp division multiplexing in millimeter-wave fiber-wireless integrated systems for enhanced mobile broadband and ultra-reliable communications," in *Proc. Opt. Fiber Commun. Conf. (OFC)*, Los Angeles, CA, USA, 2017, pp. 1–3.
- [12] M. S. Omar and X. Ma, "Designing OCDM-based multi-user transmissions," in *Proc. IEEE Global Commun. Conf. (GLOBECOM)*, Waikoloa, HI, USA, 2019, pp. 1–6.
- [13] "F-OFDM scheme and filter design," 3GPP, Sophia Antipolis, France, Rep. R1-165425, May 2016. [Online]. Available: https://www.3gpp.org/DynaReport/TDocExMtg-R1-85-31662.htm
- [14] Evolved Universal Terrestrial Radio Access (E-UTRA); Multiplexing and Channel Coding, V12.0.0, Standard 3GPP TS 36.212, Dec. 2013.